ELSEVIER

Solar Energy Materials & Solar Cells 71 (2002) 141–152

Solar Energy Materials & Solar Cells

www.elsevier.com/locate/solmat

Nanoporous SnO_2 electrodes for dye-sensitized solar cells: improved cell performance by the synthesis of 18 nm SnO_2 colloids

S. Chappel, A. Zaban*

Department of Chemistry, Bar-Ilan University, Ramat-Gan 52900, Israel

Received 8 November 2000

Abstract

This paper reports on the synthesis of SnO_2 18 nm diameter colloidal suspension for the fabrication of nanoporous electrodes. The new suspension allows the fabrication of thick and homogeneous electrodes by simple one layer spreading; in contrast to the successive spin coating of the commonly used commercial suspension that results in a thin inhomogeneous electrode. When used in dye-sensitized solar cells, the new electrodes increase the light-to-energy conversion efficiency by a factor of 2.1 in comparison with standard commercial suspension based electrodes. The improvement is mostly the result of an increase of the photocurrent. This increase is attributed to the better electrolyte migration, and presumably also to an increase of the photoinjected electron diffusion rate in the electrode.

Keywords: Dye-sensitized solar cells; SnO_2; Nanoporous electrodes; Nanosize colloids

1. Introduction

Most dye-sensitized solar cells utilize nanoporous electrodes made from TiO_2 [1–6]. However, some applications require that the conduction band potential of the nanoporous electrode is more positive than that of TiO_2 [7–11]. SnO_2 is one of the few wide band gap semiconductors that possess this property. Its conduction band potential is approximately 0.4 V more positive than that of TiO_2 [12].

*Corresponding author. Tel.: +972-3-5317876; fax: +972-3-5351250.
E-mail addresses: zabana@mail.biu.ac.il (A. Zaban).

0927-0248/02/$ - see front matter
PII: S0927-0248(01)00050-2

Reports of dye-sensitized solar cells that are based on SnO_2 nanoporous electrodes show low conversion efficiency of light to power [7,9,13]. The low efficiency is in part related to the intrinsic properties of SnO_2. The photovoltage, for example, which is partly affected by the potential of the semiconductor bands is expected to be lower in cells that are based on SnO_2 electrodes in comparison with TiO_2-based cells [9,10,13,14]. The other reason for efficiency losses may be connected to the parameters of the nanoporous SnO_2 electrodes including, for example, the sizes of both the colloids and the sizes of the pores [7,15]. The common SnO_2 electrodes are made from a commercial SnO_2 colloidal suspension (Alfa/Aesar) that is sintered on a conductive glass [7,9,13,15,16]. The thickness of a layer made from this solution is usually limited to less than 1 μm since thicker films tend to crack. Electrodes thicker than 1 μm are usually made by successive deposition of the colloidal layer when each deposition is followed by sintering [7,9]. Thick films usually suffer from lateral inhomogeneity resulting from the sequential deposition. Moreover, in this fabrication process, each colloid experiences a different sintering duration depending on its distance from the substrate. This duration difference induces inhomogeneity perpendicular to the substrate relating to the size of the pores and the electrical conductivity.

We report here on the synthesis of a new SnO_2 colloidal suspension with which a thick nanoporous electrode can be fabricated by a single layer. The new 18 nm diameter colloids are much larger than those obtained from the commercial suspension. Electrodes made from the new colloids were tested in dye-sensitized solar cells in comparison with electrodes that were fabricated from the commercial suspension. The cells containing the new electrodes exhibit approximately 2.1 times higher light-to-energy conversion efficiency mostly due to an increase of the photocurrent. The improved performance is attributed to the pore size, the homogeneity, and the electron diffusion rate.

2. Experimental

2.1. Colloids synthesis

The nanocrystalline SnO_2 suspension was made using a commercial suspension of amorphous to weekly crystalline SnO_2 nanoparticles (Alfa/Aesar) as starting material. The modification includes three major steps: (i) dilution of the original basic medium in different acids or bases, (ii) hydrothermal treatment, and (iii) recovery of the resulting nanocrystals. The original suspension of pH 9.5 (potassium ions) was diluted using analytic acetic acid, pH 1.2 nitric acid, pH 11.5 NaOH, and water. The solutions were stirred vigorously for 6 h. The hydrothermal treatment was performed in a titanium autoclave (Parr instruments) at various temperatures (200–280°C) over different time periods. The hydrothermal experiments were conducted in series of five comparable samples that varied by the dilution extent. All five samples were autoclaved together using a special Teflon setup fabricated for this purpose. Following the hydrothermal treatment, the nanocrystals were separated from the

solution and washed with extra pure water until the desired pH was achieved. Finally, the solution was sonicated to yield a homogenous suspension of SnO_2 nanocrystals.

The preparation described above yielded different colloid sizes and quality. The best suspension for the fabrication of the nanoporous dye-sensitized electrodes was made in the following way: The original suspension was diluted with acetic acid to a ratio of 1 : 11 and stirred vigorously for 6 h. The hydrothermal treatment was performed at 250°C for 4 days, followed by successive washing with extra pure water until pH 2 was obtained. Finally, the solution was sonicated to yield a homogenous suspension of 18 nm SnO_2 crystals.

2.2. Colloid characterization

X-ray diffraction patterns were used to determine the identity and crystallite size of each colloidal set. The powder XRD patterns were recorded using an X-ray diffractometer (Rigaku 2028) with Cu K_α radiation. The average crystallite size of the powders was calculated by the Scherrer formula [17]. Surface area measurements of the powders were conducted with a standard BET surface area analyzer (Micromeritics Gemini III 2375). TEM imaging and electron diffraction were carried out with a JEOL-JEM 100SX microscope, operating at 120 kV. Samples for TEM analysis were prepared by dispersing the SnO_2 onto TEM copper grids coated with thin amorphous carbon.

2.3. Nanoporous SnO_2 electrodes

Two SnO_2 suspensions were used to fabricate the nanoporous electrodes: A commercial 15% colloidal dispersion of particles in water from Alfa/Aesar and a suspension of the 18 nm diameter colloids synthesized as described above. Both electrodes were made on an F-doped SnO_2 conducting glass (Libby Owens Ford, 8 Ω/square) that were cleaned with soap, washed several times with extra pure water, and dried with condensed air.

Ten electrodes of different thicknesses were made from the commercial suspension by successive spin coating (1–10 layers of the nanoporous SnO_2). A 100 μl aliquot of the SnO_2 colloidal solution was spin coated onto each electrode at 3000 rpm followed by 15 min sintering in air at 450°C. For multilayers electrodes, heating at 450°C for 15 min followed each layer application. The electrodes fabricated from the modified suspension were fabricated as a single layer. The SnO_2 colloid paste was spread over the substrate with a glass rod using adhesive tape as spacers. The films were then fired at 450°C for 15 min in air, which resulted in films having a thickness up to 4 μm. The thickness of the film was varied by changes in the thickness of the spacers.

The dye (cis-di(isothiocyanato)-N-bis(4,4′-dicarboxy-2,2′-bipyridine) rutheniu-m(II)) (Solaronix SA) was adsorbed by immersing the electrodes overnight in a 0.5 mM dry ethanol solution. The relative amount of dye adsorbed on the electrode was calculated from its absorption spectra measured on a Hewlett-Packard 8453

spectrophotometer using an undyed nanocrystalline SnO_2 electrode as a reference. The film thickness was measured with a profilometer (Mitutoyo, Surftest SV 500).

2.4. Cell characterization

A sandwich-type configuration was employed to measure the performance of the dye-sensitized solar cell. The counter electrode, Pt coated on F-doped SnO_2 conducting glass, was distanced from the nanoporous electrode by 50 μm using two Teflon bands. The electrolyte used was 0.5 M LiI/0.05 M I_2 in a 1 : 1 mixture of dry acetonitrile and NMO. Illumination of the cell was performed using a Xe lamp calibrated to 1 sun in the 350–800 nm region. An Eco Chemie potentiostat was used to measure the photocurrent and photovoltage.

3. Results and discussion

In this paper we compare two sets of SnO_2 nanoporous electrodes and dye-sensitized solar cells containing these electrodes. The difference between the two electrode sets is the type of colloids used to fabricate these sets. In the first set, electrodes were fabricated by common spin coating procedure using the commercial suspension of amorphous SnO_2 colloids as received from the manufacturer. They are denoted as the commercial nanoporous electrodes (CNEs). The CNEs are compared with electrodes that were made by spreading a single layer of the new suspension of 18 nm diameter colloids. The suspension was synthesized using the commercial material as a starting material. The size of the new colloids matched the standard size used in most dye-sensitized solar cells. These electrodes are denoted as the synthesized nanoporous electrodes (SNEs). The difference between the two electrode types relates to several issues. We will discuss the properties of the individual colloid of each of the two types, the electrode fabrication process, and the influence of the colloid properties on the properties of the electrodes when used in dye-sensitized solar cells.

Fig. 1 presents the X-ray diffractograms of the commercial colloids as received (dried at 100°C), and after 45 min sintering at 450°C and 700°C, the crystal structure of the colloids is cassitarite. Fig. 2 presents the corresponding TEM pictures. The parameters of the colloids are summarized in Table 1. The average colloid sizes calculated from the X-ray diffractograms by the Scherrer formula are 4.05, 4.5 and 5.7 nm for the presintered colloids and after sintering at 450°C and 700°C, respectively. The TEM pictures of the commercial colloids show the same trend. As received, the material does not have a defined shape (Fig. 2a) turning into defined colloids only after sintering at 700°C (Fig. 2c). Counting 200 particles in the TEM pictures, the average size of the presintered material was measured to be 3.3 ± 0.65 nm. After sintering to 400°C and 700°C their size changed to 3.7 ± 0.6 and 5.9 ± 0.9 nm, respectively. The correlation between the crystallites' average sizes calculated from the XRD data and the colloids' sizes measured from the TEM pictures indicates that most colloids consist of single crystals. The surface area of the

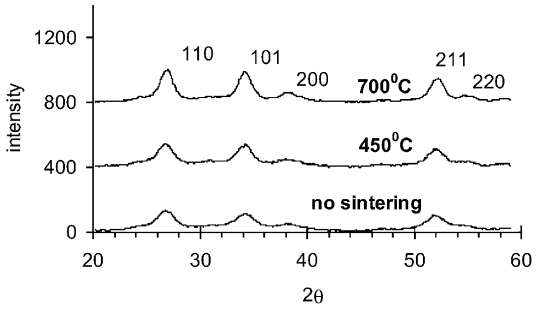

Fig. 1. X-ray diffractograms of the commercial colloids as received and after 45 min sintering at 450°C and 700°C. The sizes calculated from the diffractograms are summarized in Table 1.

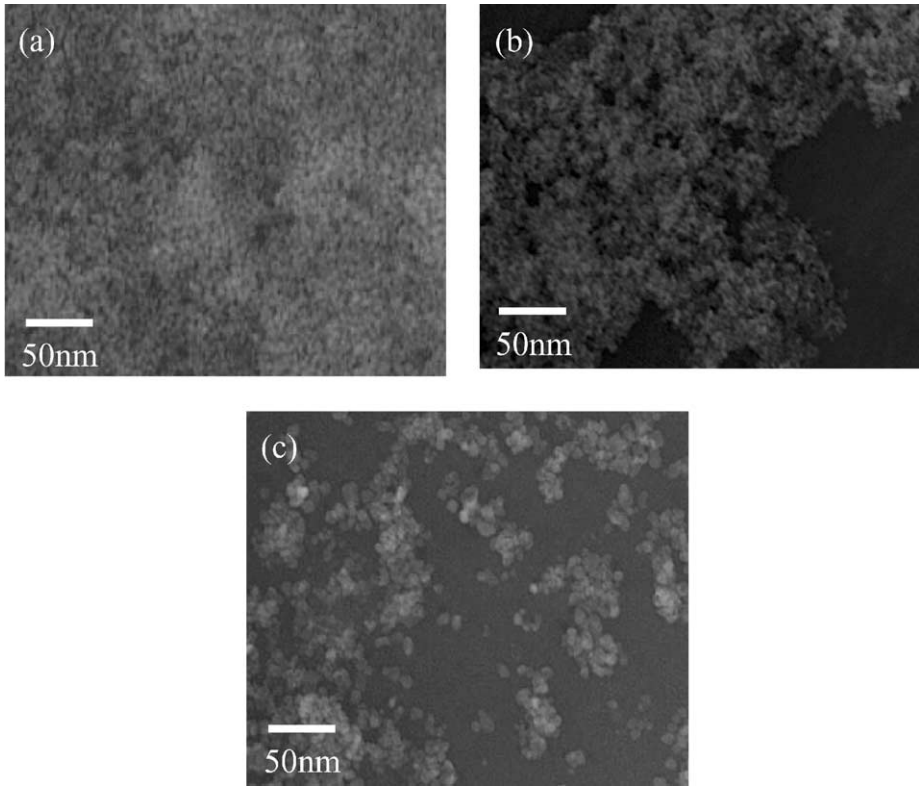

Fig. 2. TEM pictures of the commercial colloids as received and after 45 min sintering at 450°C and 700°C. The sizes measured from the pictures are summarized in Table 1.

colloids measured with BET changed from 220 m^2/g for the original commercial solution to 170 m^2/g upon sintering to 700°C.

The properties of the new colloids synthesized in this work are summarized in Figs. 3 and 4 and in Table 1. Figs. 3a and 4a show that polycrystalline material

Table 1
The average colloids' sizes and their surface areas in their primary suspension and after sintering at 450°C and 700°C. The sizes were calculated from the X-ray diffractogram line broadening using the Scherrer formula and by counting 200 particles in the TEM pictures. The surface area was measured by BET

	Commercial colloids			New colloids		
	As received	450°C	700°C	Hydrothermal treatment	450°C	700°C
Average size—XRD (nm)	4.05	4.5	5.72	17.95	18.05	23.7
Average size—TEM (nm)	3.3 ± 0.65	3.7 ± 0.6	5.9 ± 0.9	18 ± 6.2	18.6 ± 6.7	27.5 ± 7.7
Surface area—BET(m^2/g)	220		170	60		15
Crystal structure	Cassitarite			Cassitarite		

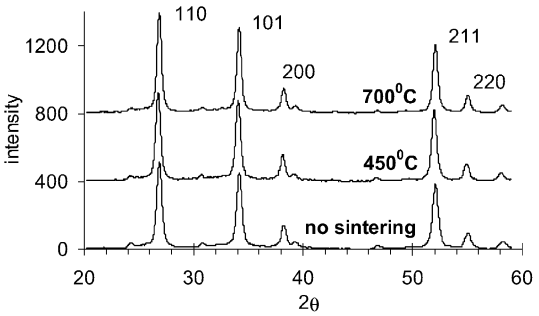

Fig. 3. X-ray diffractograms of the new colloids as received and after 45 min sintering at 450°C and 700°C. The sizes calculated from the diffractograms are summarized in Table 1.

results from the hydrothermal synthesis. Table 1 provides a summary of the nanoparticles' average sizes, which were obtained from the XRD and the TEM measurements. The average values after sintering at 450°C and 700°C are also provided. From Table 1 we can see that upon sintering to these temperatures, the size of the colloids increases to 24 nm at 700°C. Here also, the correlation between the sizes obtained from the XRD and the TEM measurements indicate that the colloids do not consist of several crystallites. The surface areas of the colloids after the hydrothermal process and sintering at 700°C (Table 1) show the same trend of increase in the colloid size during the sintering.

Large colloids were obtained only when analytic acetic acid was used to dilute the commercial suspension at a ratio of 1 : 11 prior to the hydrothermal process. Fig. 5 presents the colloid sizes that were obtained when analytic acetic acid, pH 1.2 nitric acid, water and pH 11.5 NaOH solutions were used to dilute the commercial suspension. Fig. 5 indicates that the size increase is specifically related to the acetic acid and not to acidity or dilution in general. In other words, when the concentration of the acetic acid was high enough to almost neglect the original solution the maximum crystal size was obtained. The chemistry of the process may be related to

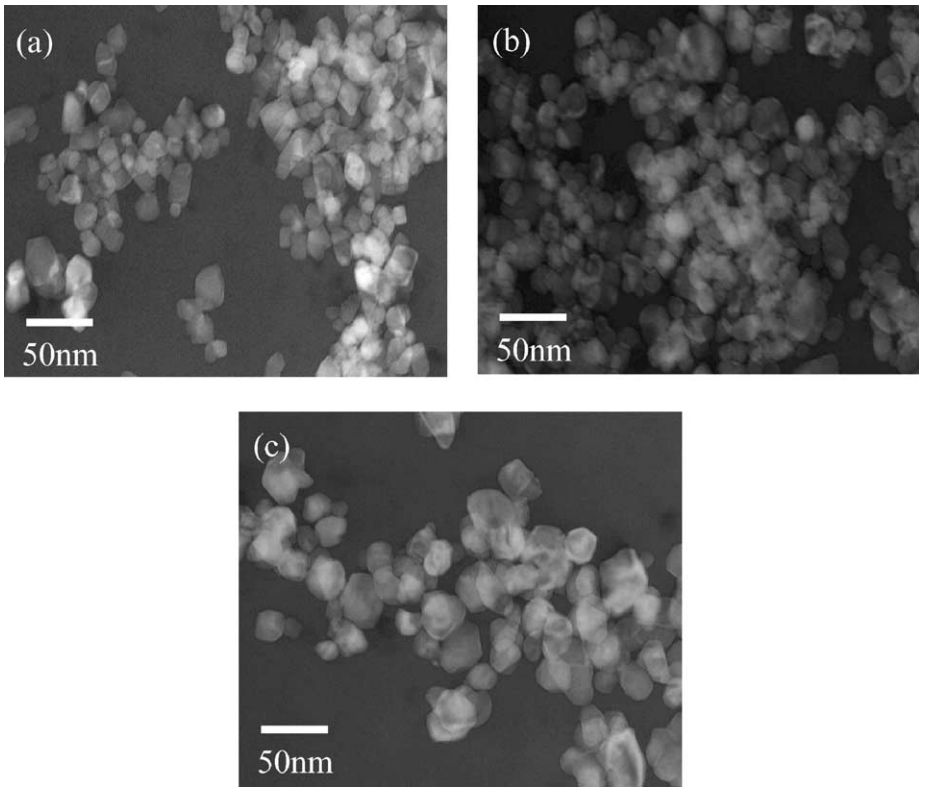

Fig. 4. TEM pictures of the new colloids as received and after 45 min sintering at 450°C and 700°C. The sizes measured from the pictures are summarized in Table 1.

the possible formation of complexes between the acetic acid and the amorphous SnO_2 or the non-reacted Sn ions [18]. However, exploring the exact mechanism of this process is beyond the scope of this work.

Another synthetic issue relates to the duration of the hydrothermal process. Fig. 6 shows that most of the size increase occurs during the first 24 h of autoclaving, after which only a small change in the crystallite sizes is measured (tests up to 3 weeks show that the growth apparently ceases entirely after 4 days). Here also, the exact mechanism was not explored, but this result indicates that the growth of the crystals is mostly via condensation of free ions or small colloids that are consumed during the first 24 h of the process.

The common method to prepare nanoporous electrodes from colloidal suspensions involves the spreading of the suspension layer on a conductive substrate using 50–150 μm spacers. After air drying the thin layer, the electrode is annealed in air, in order to form an electrical contact between the various colloids and between the colloids and the substrate. This method was adopted for the formation of the SNEs. Hence relatively thick electrodes up to 4 μm were obtained in a single process. These

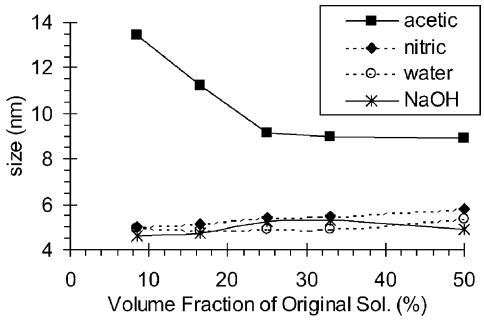

Fig. 5. The colloid sizes resulting from the hydrothermal treatment as a function of the dilution percent in various media: (a) analytic acetic acid, (b) pH 1.2 nitric acid, (c) distilled water and (d) pH 11.5 NaOH.

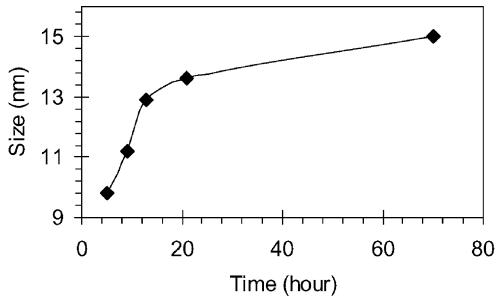

Fig. 6. The colloid average size resulting from the hydrothermal treatment in analytic acetic acid as a function of the treatment duration. As shown, most of the size increase occurs at the first 24 h of the process.

transparent, crack-free electrodes were homogeneous with respect to both the lateral and the perpendicular axes. In contrast to the SNEs, the formation of the CNEs by this method resulted in a cracked inhomogeneous film that tended to peel off the surface when sintered at high temperatures. The only way to fabricate a reasonable electrode from the commercial suspension involved successive spin coating and sintering of very thin layers. The resulting electrodes were not laterally homogeneous and were limited to small areas and low thicknesses. As mentioned above, the successive sintering is expected to induce additional inhomogeneity perpendicular to the substrate due to the different sintering duration to which each layer is exposed. The inability to fabricate a thick nanoporous layer from the commercial suspension is attributed to the small size of the colloids and to their amorphous structure. We examined a possible influence of the suspension composition with respect to the film fabrication by the replacement of the solution to various acidic media. However, we found that the suspension composition had no significant effect on the resulting film.

Fig. 7 presents the peak absorption (530 nm) of dyed nanoporous electrodes of various thicknesses that were made from the two suspensions. The linear correlation between the dye absorption and the film thickness shows that per film thickness, the

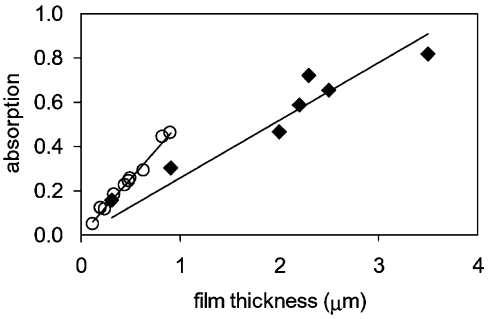

Fig. 7. The peak absorption (530 nm) of dyed nanoporous electrodes from the two suspensions as a function of the film thickness. The linear correlation is related to the surface per film thickness obtained by each colloid type.

amount of dye adsorbed to the CNEs, is twice as high as the amount attached to the SNEs. This value correlates well with the calculated 2.2 ratio of surface area per thickness. The calculation was based on the average colloid size after the 450°C sintering process (as noted in Table 1) assuming spherical colloidal shape. The correlation between the measured and calculated ratios indicates that the dye surface concentration is similar for both electrode types.

Fig. 8 presents a performance comparison with respect to the short-circuit photocurrent (J_{sc}), the open-circuit photovoltage (V_{oc}), the fill factor (FF) and the maximum power drawn from the cell (P_{max}), under 1 sun illumination. Since the electrodes fabricated from the two suspensions exhibit different surface area per thickness, the comparison is made as a function of the amount of light absorbed by the adsorbed dye in each cell. Fig. 8a shows that the photocurrent generated by the cells containing the SNEs is 2.4 times higher than the photocurrent generated by the cells containing the CNEs. This finding underestimates the improvement inherent in the SNEs, since the electrodes are compared at similar light absorption which means that the SNE is thicker than the CNE. In other words, if the SNE and the CNE were of the same thickness, requiring similar mean electron diffusion length, we would expect the SNE photocurrent to improve by more than the 2.4 factor. In both cell types, the photovoltage is similar for a given light harvesting, and the photovoltage decreases with the increase of electrode thickness. Such a decrease is often observed, and is attributed to photoelectron losses at a distance from the current collector [19]. The fill factor per light absorption is similar for both cell types, although the photocurrent obtained from the SNE based cells is higher. The overall result is approximately 2.1 higher power that is generated from the cells containing the SNEs per the same amount of dye present in the cell.

The data presented in Fig. 8 shows that the superiority of the SNEs in terms of the maximum power that is generated in the cell is mostly attributed to the photocurrent increase. This increase may be the result of the improved performance of the SNE in the following three processes: Electron injection, electron collection, and electrolyte migration. However, the results presented in Fig. 8b show that there is no electron

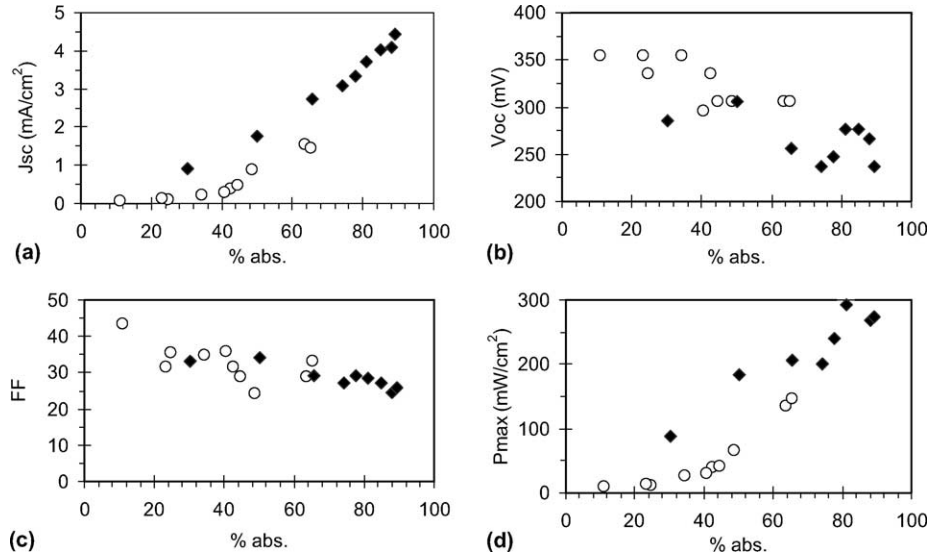

Fig. 8. Performance comparison between dye-sensitized solar cells containing the two electrode types (CNE = circles and SNE = diamonds): (a) short-circuit photocurrent, (b) open-circuit photovoltage, (c) fill factor and (d) maximum power drawn from the cell. The measurements were done at 1 sun illumination condition, as a function of the amount of light absorbed by the dye in each cell.

injection improvement for the SNEs; thus, it is mostly the electron collection efficiency and the electrolyte migration that contribute to the current increase. We base this finding on the fact that there is no significant difference in the photovoltage between the two cell types. In other words, improved injection efficiency should be reflected in an increase of the photovoltage, provided that the recombination rate in the case of the SNEs is lower or similar to that of the CNEs (which is the case here based on Figs. 8a and 8c).

Incident photon to current efficiency (IPCE) measurements provide additional support concerning the observation of improved collection efficiency. In these measurements, two cells containing the two electrode types loaded with the same amount of dye are compared. The curves of both cells resemble the absorption spectrum of the dye. Throughout the visible spectrum, the IPCE values of the SNE-based cell are higher than the values of the cell containing the CNE. However, the improvement in the conversion efficiency is wavelength dependent, as indicated by the ratio between the IPCE values of the two cells (the improvement factor). Fig. 9 shows that this factor increases at illumination wavelengths in which the absorption coefficient of the dye decreases. The wavelength dependence of the improvement factor can be directly related to the electron collection efficiency [20]. The mean distance a photoinjected electron must diffuse in order to reach the current collector increases as the absorption coefficient of the dye decreases; thus, changing the light absorption profile. This phenomenon means that recombination events are expected

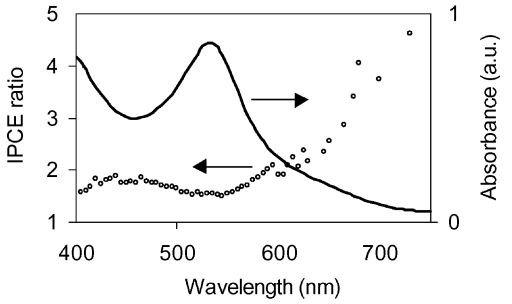

Fig. 9. The ratio between the IPCE values of the two cells (SNE/CNE) showing an increase at illumination wavelengths in which the absorption coefficient of the dye decreases.

to increase, as the absorption coefficient of the dye decreases [20]. In other words, a change in the rate of recombination is expected to have a more significant effect in the low dye absorption coefficient regions. Fig. 9 indicates that this is the case for the SNE.

The results presented in Figs. 8 and 9 lead to the following reasoning concerning the superiority of the SNEs: The SNEs allow faster migration of the electrolyte. This improves the rate of oxidized dye regeneration, and reduces the recombination rate of electrons with oxidized dye or oxidized ions in the solution. In addition, we speculate that the electron diffusion in the SNEs is faster, thus increasing the photocurrents, although at this point we are unable to provide a clear proof. Faster electron migration may result from a decrease of the trapping concentration or depth [21–23], especially those that are related to surface states, or from improved electrical conductivity that is expected when larger colloids are sintered to each other [24,25]. Further experiments concerning these issues are currently under investigation.

4. Conclusions

The synthesis of a SnO_2 colloidal suspension for the fabrication of nanoporous electrodes is reported. Unlike commonly used 4 nm commercial colloids, the new SnO_2 suspension contains 18 nm colloids. This SnO_2 suspension enables the fabrication of thick and homogeneous electrodes by simple spreading. This process is in contrast to the successive spin coating of the commercial suspension that results in a thin inhomogeneous electrode.

Comparing the new electrodes (SNEs) with the standard ones (CNEs) resulted in a significant 2.1 times improvement of light-to-energy conversion efficiency. We note that a photocurrent increase is the primary cause for this improvement. We attributed this increase to both the better electrolyte migration and an apparent increase of the photoinjected electron diffusion rate in the electrode.

Acknowledgements

This research was supported by The Israel Science Foundation founded by The Israel Academy of Science and Humanities.

References

[1] T. Gerfin, M. Gratzel, L. Walder, Molecular and supermolecular surface modification of nanocrystalline TiO_2 films: charge separating and charge injecting devices, in: K.D. Karlin (Ed.), Molecular Level Artificial Photosynthetic Materials, Vol. 44, Wiley, Inc., New York, 1997, p. 345.
[2] A. Hagfeldt, B. Didriksson, T. Palmqvist, H. Lindstrom, S. Sodergren, H. Rensmo, S.E. Lindquist, Sol. Energy Mater. Sol. Cells 31 (1994) 481.
[3] M.K. Nazeeruddin, P. Pechy, M. Gratzel, Chem. Commun. 18 (1997) 1705.
[4] B. O'Regan, M. Gratzel, Nature 353 (1991) 737.
[5] F. Cao, G. Oskam, P.C. Searson, J. Phys. Chem. 99 (1995) 17071.
[6] N.G. Park, G. Schlichthorl, J. van de Lagemaat, H.M. Cheong, A. Mascarenhas, A.J. Frank, J. Phys. Chem. 103 (1999) 3308.
[7] S. Ferrere, A. Zaban, B.A. Gregg, J. Phys. Chem. B 101 (1997) 4490.
[8] S. Ferrere, B.A. Gregg, J. Amer. Chem. Soc. 120 (1998) 843.
[9] P.V. Kamat, I. Bedja, S. Hotchandani, L.K. Patterson, J. Phys. Chem. 100 (1996) 4900.
[10] K. Sayama, H. Sugihara, H. Arakawa, Chem. Mater. 10 (1998) 3825.
[11] P.V. Kamat, S. Barazzouk, K.G. Thomas, S. Hotchandani, J. Phys. Chem. B 104 (2000) 4014.
[12] A.J. Nozik, R. Memming, J. Phys. Chem. 100 (1996) 13061.
[13] K. Tennakone, G. Kumara, I.R.M. Kottegoda, and V.P.S. Perera, Chem. Commun. (1999) 15.
[14] S. Burnside, J.E. Moser, K. Brooks, M. Gratzel, D. Cahen, J. Phys. Chem. B 103 (1999) 9328.
[15] W.E. Ford, J.M. Wessels, M.A.J. Rodgers, J. Phys. Chem. B 101 (1997) 7435.
[16] G. Boschloo, D. Fitzmaurice, J. Phys. Chem. B 103 (1999) 3093.
[17] B.D. Cullity, Elements of X-Ray Diffraction, Addison-Wesley, Inc., London, 1978.
[18] J. Livage, M. Henry, C. Sanchez, Prog. Solid State Chem. 18 (1998) 259.
[19] J. van de Lagemaat, N.G. Park, A.J. Frank, J. Phys. Chem. B 104 (2000) 2044.
[20] G. Hodes, I.D.J. Howell, L.M. Peter, J. Electrochem. Soc. 139 (1992) 3136.
[21] J. Nelson, Phys. Rev. B 59 (1999) 15374.
[22] N.W. Duffy, L.M. Peter, K.G.U. Wijayantha, Electrochem. Commun. 2 (2000) 262.
[23] J. van de Lagemaat, A.J. Frank, J. Phys. Chem. B 104 (2000) 4292.
[24] A. Zaban, S.T. Aruna, S. Tirosh, B.A. Gregg, Y. Mastai, J. Phys. Chem. B 104 (2000) 4130.
[25] S.T. Aruna, S. Tirosh, A. Zaban, J. Mater. Chem. 10 (2000) 2389.